Sarakorn and Vachiratienchai
Earth, Planets and Space (2018) 70:103
https://doi.org/10.1186/s40623-018-0876-7

Earth, Planets and Space

FULL PAPER

Open Access

Hybrid finite difference–finite element method to incorporate topography and bathymetry for two-dimensional magnetotelluric modeling

Weerachai Sarakorn[1*] and Chatchai Vachiratienchai[2]

Abstract

In this research, a new numerical method, called the hybrid finite difference–finite element (hybrid FD–FE) method, is developed to solve 2-D magnetotelluric modeling by taking advantage of both the finite difference (FD) and finite element (FE) methods. With the hybrid FD–FE method, the model is first discretized as rectangular blocks and separated into two zones: the FD and FE zones. The FD zone is set for the subregions where topography or bathymetry does not appear. The FD approximation, which is fast, accurate and requires less memory resources, is then applied. For the FE zones where topography or bathymetry exists, the rectangular blocks are transformed into quadrilateral elements to handle the topography or bathymetry appropriately. Then, the FE approximation with quadrilateral elements, which is more accurate for topography or bathymetry zones, is applied. The system of equations for the hybrid FD–FE method is then formed according to the FD and FE schemes. The obtained system is a combination of the FD and FE equations. Three numerical methods are applied to test models with and without topography and bathymetry. The accuracy and efficiency in terms of errors, computational time and memory storage are presented, compared and discussed. The numerical experiments indicate that the FD scheme has a shorter computational time than the other schemes when modeling without topography and retains accuracy equivalent to that of the FE method, whereas FE is more practical when modeling with topography and bathymetry. However, our proposed hybrid FD–FE method is efficient in both situations. Without topography or bathymetry, its efficiency and accuracy approach those of the FD scheme. With topography and bathymetry, the hybrid FD–FE method is as accurate as FE, but its speed is slightly slower than that of FD. In terms of memory storage, the hybrid FD–FE method consumes slightly more storage than the FD method. This hybrid FD–FE method can be further extended and implemented for 3-D magnetotelluric modeling for more efficient computation.

Keywords: Hybrid method, Finite difference method, Finite element method, 2-D magnetotelluric modeling

Mathematics Subject Classification: 65*N*30, 65*N*50, 74*S*05

Introduction

Topography or bathymetry zones may be encountered during magnetotelluric surveys. These zones can affect the apparent resistivity and phase obtained from two-dimensional magnetotelluric (MT) surveys (Schwalenberg and Edwards 2004; Wannamaker et al. 1986). On land, a ridge causes a low apparent resistivity zone beneath it, whereas its foothill causes a high resistivity zone. These effects are observed in the transverse electric (*E*-polarization) and transverse magnetic (*H*-polarization) modes. However, the effects of a ridge on the apparent resistivity are greater for *E*-polarization than for *H*-polarization. The effects of the ridge on the phase are similar to the effects on the apparent resistivity for both *E*- and *H*-polarizations. Furthermore, the effects

*Correspondence: wsarakorn@kku.ac.th
[1] Department of Mathematics, Faculty of Science, Khon Kaen University, Khon Kaen 40002, Thailand
Full list of author information is available at the end of the article

of a ridge also depend on the period of the EM field to be considered. The effects of a ridge are greater in a short period and reduced for longer periods. The effect of a valley on land is opposite that of a ridge. Beneath the sea, the effects of ridges and valleys on the responses calculated for both the *E*- and *H*-polarizations are the converse of those calculated on land. These effects can result in misleading interpretations but can be corrected with some techniques (Baba and Chave 2005; Matsuno et al. 2007; Nam et al. 2008; Singer 1992). These techniques are approximations and yield numerical errors. Therefore, the appropriate incorporation of topography and bathymetry with less consumption of memory storage and computation time during modeling is necessary to avoid these artifacts and to enable efficient forward modeling for the inversion process.

Finite difference (FD) and finite element (FE) methods are mostly developed and applied as the main process of forward calculation for 2-D and 3-D inversions (Egbert and Kelbert 2012; Franke et al. 2007; Key and Weiss 2006; Kordy et al. 2016a, b; Lee et al. 2009; Mackie et al. 1993; Nam et al. 2007; Ren et al. 2013; Sarakorn 2017; Sharma and Kaikkonen 1998; Siripunvaraporn et al. 2002; Usui 2015; Usui et al. 2017, 2018; Wannamaker et al. 1986, 1987). The FD method is accurate for simple modeling and, because of the limitation of the structured rectangular mesh, consumes less memory storage and computation time. The FE method is accurate for real-world complex modeling, especially topography and bathymetry, because of the greater flexibility of mesh schemes (Franke et al. 2007; Grayver and Kolev 2015; Grayver 2015; Key and Weiss 2006; Kordy et al. 2016a, b; Lee et al. 2009; Nam et al. 2007; Ren et al. 2013; Sarakorn 2017; Sharma and Kaikkonen 1998; Usui 2015; Usui et al. 2017, 2018; Wannamaker et al. 1986, 1987). However, the disadvantages of FE are greater consumption of memory storage and longer computation time. Thus, combining these two methods to exploit their advantages for solving magnetotelluric modeling is of interest and a challenge.

In this paper, we present a hybrid finite difference–finite element method (or hybrid FD–FE method, abbreviated HB) to incorporate topography and bathymetry for 2-D magnetotelluric modeling. The rectangular blocks around the topography (or bathymetry) zone are transformed to quadrilateral elements to perform FE approximation, whereas the FD approximation is performed outside. The system of equations for the hybrid FD–FE method is a combination of the FD and FE systems of equations. FE is mostly used only around the topography zone. Otherwise, the FD method is applied, and the hybrid FD–FE system of equations is, therefore, closer to the FD system of equations. For the same mesh, the computational time of hybrid FD–FE is, thus, closer to that of FD, whereas the accuracy of the hybrid FD–FE method is the same as that of FE.

Within the scope of this work, we begin by reviewing the 2-D magnetotelluric governing equation. Then, the processes of the common FD and FE methods are described, and a theoretical comparison of these methods is discussed. Next, the compatibility conditions between the FD and FE methods are confirmed to construct the hybrid FD–FE scheme. Then, the main concept of the hybrid FD–FE method for 2-D magnetotelluric forward modeling is introduced and explained in detail, and the validity of the hybrid method is confirmed with numerical experiments. Here, the simple automatic mesh algorithm used for these experiments is introduced. Next, the accuracy in terms of relative errors and efficiency in terms of computation time and consumption of memory resources of the hybrid FD–FE method on both nontopographic or nonbathymetric models and topographic or bathymetric models are presented and discussed in comparison with those of the common FD and FE methods. Finally, some conclusions and important remarks are given.

Two-dimensional magnetotelluric modeling

Governing equations

For MT modeling, the natural electromagnetic (EM) wave usually acts as a plane wave and harmonic diffusion. In addition, the displacement currents are neglected and the time-dependent $e^{-i\omega t}$ is assumed, where t is time and ω is an angular frequency ($\omega = 2\pi/T$, T is a period). Assuming a strike direction that parallels the x- direction, i.e., $\rho = \rho(y, z)$, the governing equation, in general form, is given by

$$\frac{\partial}{\partial y}\left(a\frac{\partial \phi}{\partial y}\right) + \frac{\partial}{\partial z}\left(a\frac{\partial \phi}{\partial z}\right) + b\phi = 0. \tag{1}$$

The coefficients a and b and the variable ϕ are notations that depend on the two polarizations:

$$E\text{-polarization:} \quad \phi = E_x, \quad a = 1, \quad b = i\omega\mu_0/\rho, \tag{2}$$

$$H\text{-polarization:} \quad \phi = H_x, \quad a = \rho, \quad b = i\omega\mu_0, \tag{3}$$

where E_x and H_x are the electric and magnetic fields in the x-direction, respectively, and μ_0 is the magnetic permeability in free space (Vs/Am). The bounded region D is defined by $D = D_1 \cup D_2 \cup \Gamma \cup \Gamma^{\text{int}}$, where D_1 is the air subregion, D_2 is the earth subregion, Γ is the outer boundary and Γ^{int} is the air–earth interface, where the electrical conductivity ρ is discontinuous. An example of domain D with terrain is shown in Fig. 1 (top).

The governing equation (1) is subjected to the Dirichlet boundary conditions

$$\phi = \phi_0(y,z) \quad \text{on} \quad \Gamma, \tag{4}$$

where $\phi_0(y,z)$ is approximated by solving the one-dimensional MT modeling. The solution to (1) can be treated using analytical methods if the D_2 or earth subdomain includes some simple subregions such as halfspace, horizontal layered, simple topography and bathymetry interfaces (Schwalenberg and Edwards 2004). However, numerical methods are practical and appropriate when some complex subregions and irregular interfaces appear in the model.

Hybrid finite difference–finite element method

Finite difference method

The FD method is a well-known numerical scheme that is used to approximate the solution of partial differential equations by estimating some derivative terms in the discrete difference equations. To briefly describe the procedure of the FD scheme for treating (1), let us consider a given resistivity model with some terrains, shown in Fig. 1 (top). For the first step, the given continuous model is discretized or meshed into rectangular blocks. With the limitation of rectangular grids, some topography or bathymetry appearing in the model with slope cannot be handled perfectly. Consequently, some slopes need to be truncated into many steps. The discretized model is shown in Fig. 1 (left bottom). Then, the governing equation in (1) is transformed to the difference equations, and its derivative terms are approximated by using the central difference. The obtained difference equation at node (i,j) is given by

$$A_T^{ij}\tilde{\phi}_{i,j-1} + A_L^{ij}\tilde{\phi}_{i-1,j} + A_C^{ij}\tilde{\phi}_{i,j} + A_R^{ij}\tilde{\phi}_{i+1,j} + A_B^{ij}\tilde{\phi}_{i,j+1} = 0, \tag{5}$$

where A_T^{ij}, A_L^{ij}, A_R^{ij} and A_B^{ij} are the coefficients between the central node (i,j) and the top node $(i,j-1)$, left node $(i-1,j)$, right node $(i+1,j)$ and bottom node $(i,j+1)$, respectively. The remaining coefficient A_C^{ij} is a self-coefficient at node (i,j). Note that these coefficients are expressed in terms of block sizes and block resistivity. Finally, applying the Dirichlet boundary conditions obtained by solving the 1-D problem, rearranging and grouping all coefficients in (5) together, the obtained system of equations is given by

$$\mathbf{A}\tilde{\mathbf{\Phi}} = \mathbf{s}, \tag{6}$$

where the coefficient matrix $\mathbf{A}$ is sparse, symmetric and contains five bands with complex number coefficients but is not Hermitian. $\tilde{\mathbf{\Phi}}$ is the unknown interior field vector, and $\mathbf{s}$ is a source vector. Equation (6) can be solved by either a direct or iterative solver. Here, we use the direct solver for a sparse matrix in MATLAB to obtain the solution to (6). Finally, the MT responses including impedances, apparent resistivity and phases at each site for each EM period are calculated by

$$E\text{-polarization:} \quad Z_{xy} = \frac{E_x}{Hy}, \quad \rho_{xy} = \frac{1}{\omega\mu}|Z_{xy}|^2, \quad \phi_{xy} = \arg(Z_{xy}), \tag{7}$$

$$H\text{-polarization:} \quad Z_{yx} = \frac{E_y}{Hx}, \quad \rho_{yx} = \frac{1}{\omega\mu}|Z_{yx}|^2, \quad \phi_{yx} = \arg(Z_{yx}). \tag{8}$$

Quadrilateral element-based finite element method

In addition to the FD approach, the FE scheme is a powerful numerical method that is used to approximate the solution of boundary-valued problems of partial differential equations. Similar to the FD method, the FE method begins with meshing. In contrast to the FD method, the mesh algorithm for FE approximation is not restricted to only a rectangular mesh. A resistivity model can be meshed into either triangular or quadrilateral elements. Furthermore, the pattern of mesh can be designed as structured and unstructured meshes. With these enhanced features, the discrete model can handle some topography, bathymetry and irregular subregions inside the model more appropriately. This work focuses on the FE method with quadrilateral elements. An example of a quadrilateral mesh is illustrated in Fig. 2 (left). Next, the approximated solution $\tilde{\phi}$ to (1) for each quadrilateral element is expressed as a linear combination of four basis functions and unknowns at four nodes. Applying the weighted residual Galerkin's method to (1), integrating the resulting weight function over the whole domain and setting to zeros, and simplifying this for each element (i,j) and its neighbor, we obtain the discrete equation

$$B_{LT}^{ij}\tilde{\phi}_{i-1,j-1} + B_{CT}^{ij}\tilde{\phi}_{i,j-1} + B_{RT}^{ij}\tilde{\phi}_{i+1,j-1} + B_L^{ij}\tilde{\phi}_{i-1,j} + B_C^{ij}\tilde{\phi}_{i,j} + B_R^{ij}\tilde{\phi}_{i+1,j} + B_{LB}^{ij}\tilde{\phi}_{i-1,j+1} + B_{CB}^{ij}\tilde{\phi}_{i,j+1} + B_{RB}^{ij}\tilde{\phi}_{i+1,j+1} = 0, \tag{9}$$

where $B_{LT}^{ij}, B_{CT}^{ij}, B_{RT}^{ij}, B_L^{ij}, B_R^{ij}, B_{LB}^{ij}, B_{CB}^{ij}$, and K_{RB}^{ij} are the coefficients between the center node (i,j) and left-top node $(i-1,j-1)$, center-top $(i,j-1)$, right-top node $(i+1,j-1)$, left-center node $(i-1,j)$, right-center node $(i+1,j)$, left-bottom node $(i-1,j+1)$, center-bottom node $(i,j+1)$ and right-bottom node $(i+1,j+1)$, respectively, and B_C^{ij} is a self-coefficient. As with the FD approach, these coefficients are all expressed in terms of element size and element resistivity. For the last step,

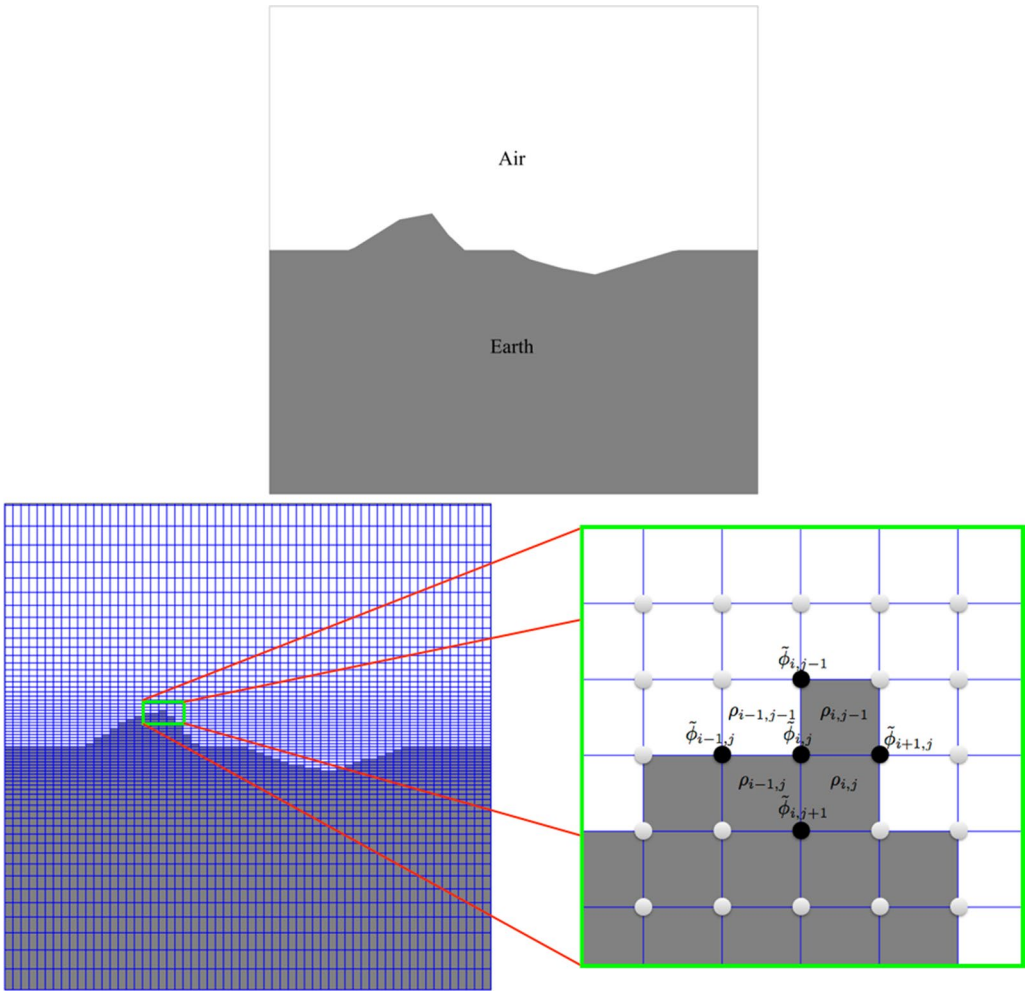

Fig. 1 The resistivity model with terrain (top). The discrete model with rectangular blocks (left bottom). The approximation of field $\tilde{\phi}$ by using the four neighbor nodes is demonstrated (right bottom)

applying Dirichlet boundary conditions and assembling coefficients and unknowns, the obtained system of equations is given by

$$\mathbf{B}\tilde{\mathbf{\Phi}} = \mathbf{s}. \tag{10}$$

The coefficient matrix **B** is large, sparse and symmetric and contains nine bands with complex number but is not Hermitian. $\tilde{\mathbf{\Phi}}$ is the unknown vector, and **s** is the source vector corresponding to the boundary conditions. As with FD, the direct solver in MATLAB is also used to solve (10). Then, the impedances, apparent resistivity and phases are finally computed at each site.

Theoretical comparison of the FD and FE methods

As shown in Figs. 1 and 2, both the FD and quadrilateral-based FE methods define electric (magnetic) fields at each node with the same coordinates. Then, the numbers of unknowns $\tilde{\phi}$ generated by the FE and FD methods are, therefore, identical when their meshes are the same. Furthermore, the coefficient matrices **A** and **B** have the same dimension. However, the matrix **A** has only five bands, whereas the matrix **B** has nine, and the number of nonzero coefficients of **A** is, therefore, less than that of **B**. Thus, the FD method requires less memory resources than the FE method. In addition, the calculation time required by the direct solver in MATLAB to solve (6) is expected to be less than that for (10).

Concept of the hybrid method

In many previous works, the solutions to (1) obtained by the FD and FE schemes are not very different when the models do not include topography and bathymetry. However, when topography or bathymetry appears in the model, the FE scheme with relaxed elements, i.e., triangular or quadrilateral elements, is more suitable for handling an interface with topography or bathymetry than

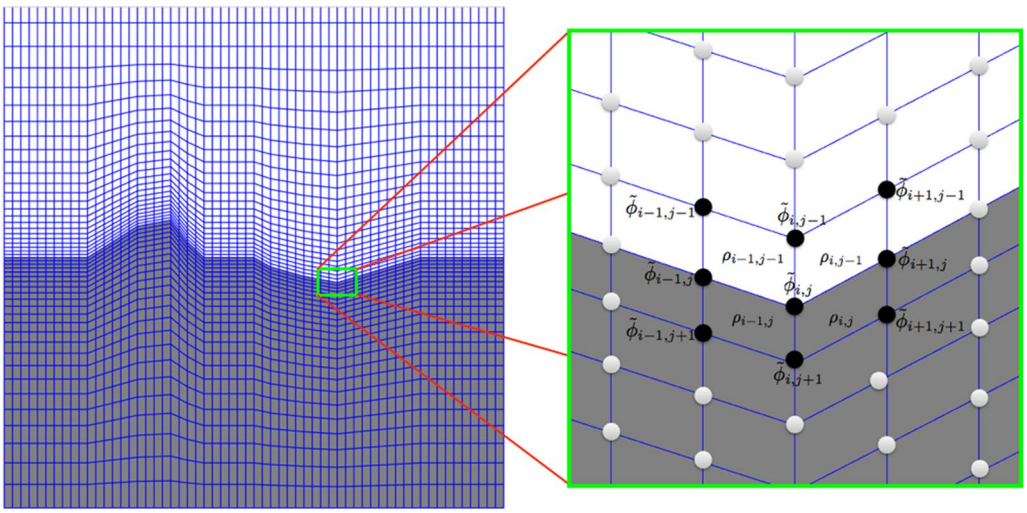

Fig. 2 The discretized model with quadrilateral elements (left). The approximation of field $\tilde{\phi}$ by using the eight neighbor nodes is demonstrated (right)

the rectangular blocks of the FD scheme. This advantage can be seen in Fig. 2. The FE method may be more accurate than FD. Evidence in support of this advantage has been provided by 2-D resistivity modeling (Erdoğan et al. 2008). For these reasons, it is interesting and challenging to introduce a hybrid FD–FE method that can combine the advantages of the FD and quadrilateral element-based FE methods while avoiding their deficiencies. Hybrid FD–FE approaches are not new and have been proposed and applied to solve various science and geoscience problems. Evidence of their applications can be found in elastic wave modeling (Galis et al. 2008; Jianfeng and Tielin 2002), hydrology (Simpson and Clement 2003) and direct current resistivity modeling (Vachiratienchai et al. 2010).

Usually, the dimensions of the systems of equations generated for the same discrete model by the FD and FE methods are identical. The obtained approximated solutions at each node should be similar. There is some evidence that the FE and FD methods provide similar discrete approximate solutions when applied to the same mesh (Zienkiewicz and Cheung 1965), supporting the construction of a hybrid method. If there are greater differences between the two approximations, then a hybrid method will require a transition zone from FE to FD or vice versa to ensure validity during modeling (Galis et al. 2008).

In this work, the hybrid FD–FE method is constructed to solve 2-D magnetotelluric modeling without any transition zone. For the application of the hybrid FD–FE method to 2-D direct current resistivity modeling (Vachiratienchai et al. 2010), the FD approach with rectangles and FE approach with right triangles are compared. The right triangles are applied on the interface where the topography is included. The hybrid FD–FE method provides good accuracy when the angle of the triangle or slope of the topography does not exceed 75°. For large-scale MT modeling, some steep terrain may appear in the model. A hybrid FD–FE approach with such a composition may cause and increase numerical errors. To avoid and prevent unpredictable errors, the hybrid FD–FE method with a conformal shape is used.

In this work, the construction of the hybrid FD–FE method begins by separating a given model into FD and FE zones. As shown in Fig. 3 (left), some FE zones are set for any topographic and bathymetric zones and optimized. Note that separated multiple FE zones can be allowed during modeling. By contrast, the FD zone is set in a simple or flat zone where topography and bathymetry do not exist. Next, the initial mesh with rectangular blocks is generated and applied in the FD zones. Then, the rectangular blocks located in the FE zones are relaxed to the quadrilateral shapes to handle topography and bathymetry appropriately. Examples of meshes for the FD and FE zones are shown in Fig. 3 (right). Note that the number of quadrilateral elements in the FE zone is equal to the initial number of rectangular blocks.

The FE and FD approximations are derived independently for their zones. Thus, the linear combination of (6) and (10) forms the single system of equations for the hybrid FD–FE method:

$$(\alpha\mathbf{A} + \beta\mathbf{B})\tilde{\phi} = \mathbf{s}, \tag{11}$$

where $\boldsymbol{\alpha}$ and $\boldsymbol{\beta}$ are the diagonal matrices such that

$$\alpha_{ii} = \begin{cases} 1 & \text{if node } i \text{ is located in the FD zone,} \\ 0 & \text{otherwise,} \end{cases}$$

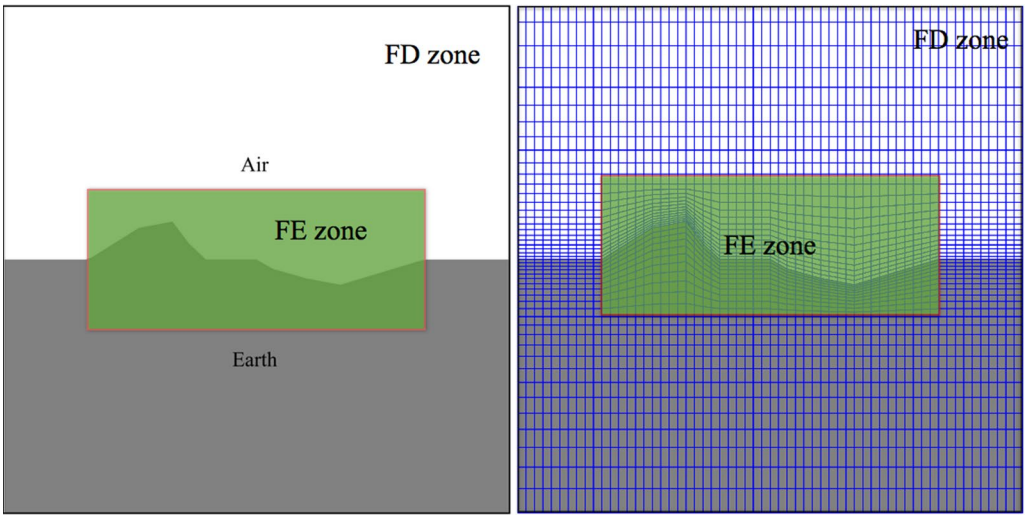

Fig. 3 The model with setting of the FD and FE zones (left). The FE zone is set and optimized for the terrain zone (light green), whereas the FD zone is set for the simple zone without terrain. Design of the mesh of the FD and FE zones (right). Quadrilateral elements are used for the FE zone, whereas rectangular blocks are used for the FD zone

and

$$\beta_{ii} = \begin{cases} 1 & \text{if node } i \text{ is located in the FE zone,} \\ 0 & \text{otherwise.} \end{cases}$$

Note that the system of equations derived by the hybrid FD–FE method in (11) is not symmetric. Note that if the FE zone is not inserted into the model, the system (11) is reduced and becomes (6). An example of a sparsity pattern resulting from the hybrid FD–FE method is shown in Fig. 4. For this case, the domain is discretized into 1378 nodes, and some FE zones are inserted into the model. Similar to the common FD and FE schemes, the direct solver in MATLAB is also used to solve (11). Consequently, the MT responses are estimated for each site.

Numerical experiments

In this section, numerical experiments are designed to investigate the accuracy and efficiency of the hybrid FD–FE method. Experiments are performed on both nontopographic and topographic models. The two-layered model is used for the nontopographic case. The topographic and bathymetric models including two models, land topographic and bathymetry models are selected as the case studies.

For each model, the mesh algorithm, which is the first process and plays an important role in both the accuracy and efficiency of the three numerical methods, needs to be considered. If the mesh generation generates a mesh with many nodes, then good accuracy is obtained, but the efficiency is worse because it requires more memory resources, such as for storing mesh data and nonzero coefficients in coefficient matrices. Furthermore, more operations are required during the formation and solution of the system of equations. In this work, the mesh algorithm used to generate the discrete model for the three numerical methods is a simple nonuniform rectangular mesh. For the case where topography or bathymetry exists in the model, the generated rectangular mesh inside those subregions is transformed into the quadrilateral mesh to handle topography or bathymetry. This transformation is only required for the FE and hybrid FD–FE methods. To generate the mesh, the lengths of the edges of consecutive blocks in the y- and z-directions are automatically generated by

$$\delta_i^p = r\delta_{i-1}, \tag{12}$$

for $i = 1, 2, 3, \ldots$, where δ_0^p is the initial length, r is the growth rate and $p = y$ or z. The upper bound of δ_i^p must be set to prevent a huge mesh size. If δ_0^p is greater than the size of some subregions or the site distance, then it is divided by an appropriate proportion. Generating the sequence in (12) for the y- and z-directions transforms the continuous model into a discrete model with rectangular blocks. Clearly, the parameters in (12) control the roughness or fineness of the mesh inside the discrete model and directly affect the number of nodes and rectangular blocks in the domain. Thus, the selection of these parameters to generate mesh data requires optimization to produce a trade-off between accuracy and efficiency. When the three numerical methods finish the task completely, the obtained numerical results are

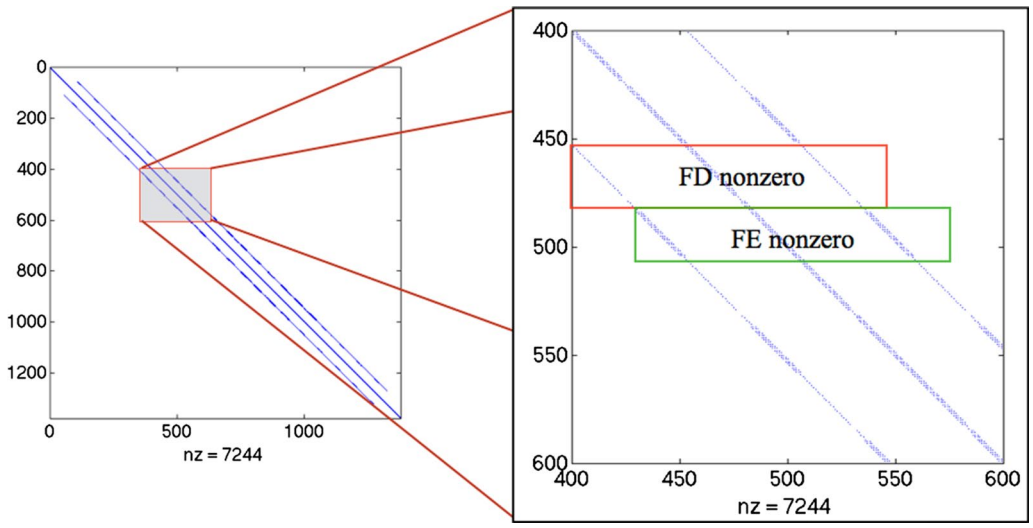

Fig. 4 Sparsity pattern in the matrix derived by the hybrid FD–FE method. The cluster of FE nonzeros is inserted in the coefficient matrix

presented, compared and discussed. Note that the computing tool used for executing FD, FE and hybrid FD–FE codes in all experiments is a MacBook Pro with CPU 2.3 GHz Core i5 and RAM 8 GB.

Nontopographic model

The two-layered model illustrated in Fig. 5 is used as an example for nontopographic case. It is supposed that the resistivity model includes two layers. The thickness of the top layer is 1 km, and its resistivity is assumed to be 100 ohm-m. For the bottom layer, its thickness and resistivity are assumed to be 99 km and 1 ohm-m, respectively. The size of the model is set as 50 km $\times$ 100 km. The total number of sites used to calculate the apparent resistivity and phase is 11 sites and those lie on the flat air–earth interface with an equal distance of 2 km. The locations of the sites are marked by red triangles. The periods of the EM field used to test this model are $T = 0.1$ and 10 s. For information for mesh generation, we set the initial mesh size $\delta_0^y = \delta_0^z = 32, 64$, and 160 m, which are approximately 1/50, 1/25 and 1/10 of the shortest penetration depth of the EM field on the top layer,

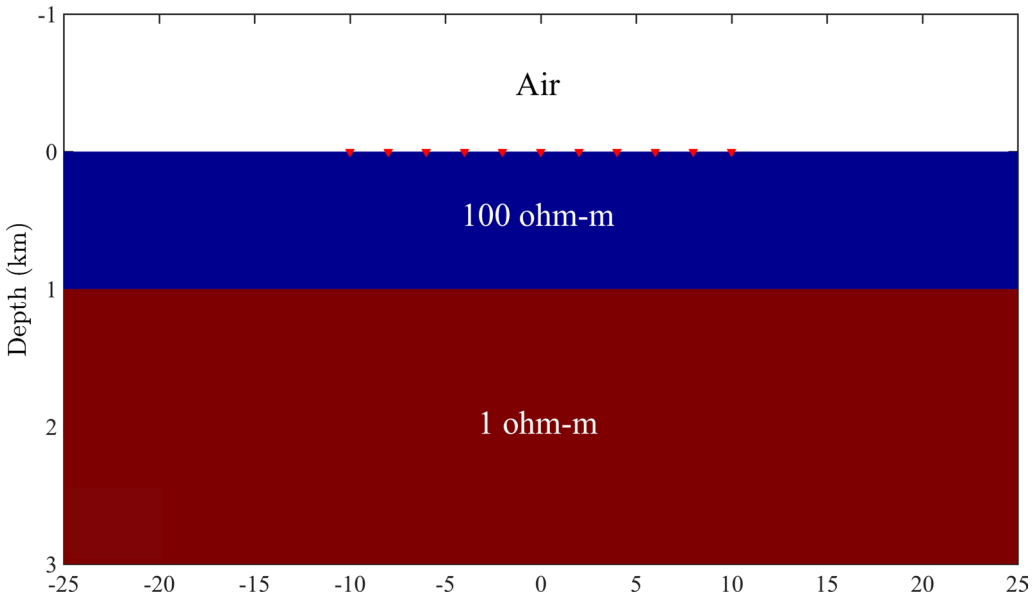

Fig. 5 The nontopographic model with two layers. The locations of the sites are marked as red triangles

respectively, and $r = 1.1, 1.2, 1.3, 1.4$. All this information is used for FD, FE and hybrid FD–FE methods. Since these are nontopographic models, the FE zone is set as the small subregion that covers all nodes on the flat air–earth interface that are in range between the first and last sites. Therefore, the accuracy of the three methods is only focused in this section. To consider the accuracy of numerical methods, we measure the relative error (%) of the apparent resistivity and phases, respectively. The obtained relative errors of the apparent resistivity (%) are shown in Fig. 6.

For all cases, the FE method provides the lowest average relative error, whereas the FD method provides the highest. The errors of the hybrid FD–FE method are closer to those of the FD method than the FE method because the FE zone is very small compared with the FD zone. The errors calculated by the FE method are approximately 1/3 those of the FD and hybrid FD–FE methods. The lowest error for each method is observed at $T = 10$ s in the case where $r = 1.1$, $\delta_0^z = 32$ m, in which the mesh of the model is finest. By contrast, the highest error for each method occurs at $T = 0.1$ s in the case where $r = 1.2$, $\delta_0^z = 160$ m. For fixed r, the error of each method increases when δ_0^z increases. For fixed δ_0^z, the error increases when r increases. Thus, both r and δ_0^z affect the accuracy of the three methods. However, δ_z^0 appears to play a significantly more important role than the growth rate. Next, the relative errors of the phases are considered and shown in Fig. 7.

The errors of the phases are less than 0.35% and small compared to those of the apparent resistivity. Similar to the errors of the apparent resistivity, the FE method is more accurate than the FD and hybrid FD–FE methods. The errors obtained by the hybrid FD–FE method are also more similar to those obtained by the FD than the FE method. The mesh parameters r and δ_0^z both still affect the accuracy of the three methods.

Topographic and bathymetric models

In this section, two more complex and realistic 2-D models with topography and bathymetry are designed and used in numerical experiments. The accuracy in terms of numerical errors is estimated, compared and discussed, whereas the efficiency in terms of CPU time and consumption of memory resources is collected, compared and discussed.

Topographic model

The first model with topography is shown in Fig. 8. There are two irregular anomalies embedded in the 100 ohm-m halfspace. The first anomaly with 1000 ohm-m is buried beneath the mountain at left, whereas the second with 1 ohm-m is buried beneath the valley at right. The bases of these anomalies are at a depth of 3 km. The top of the

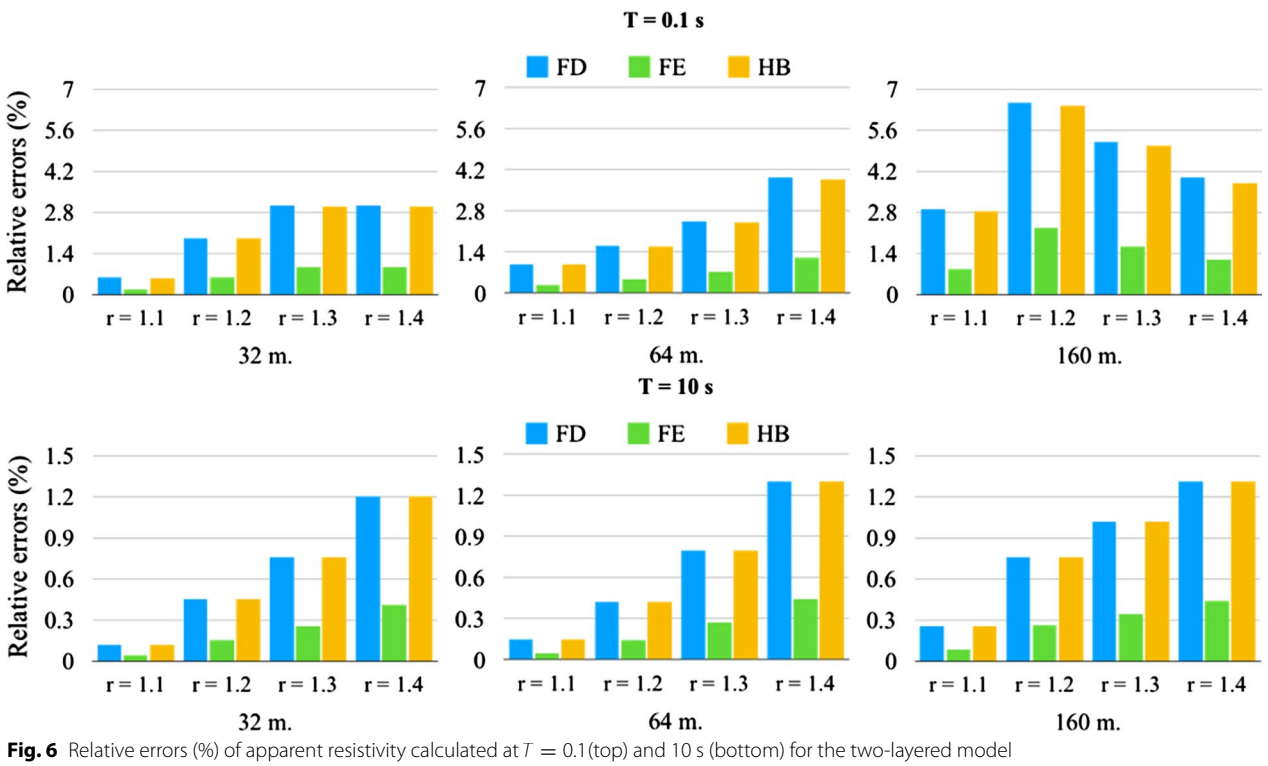

Fig. 6 Relative errors (%) of apparent resistivity calculated at $T = 0.1$ (top) and 10 s (bottom) for the two-layered model

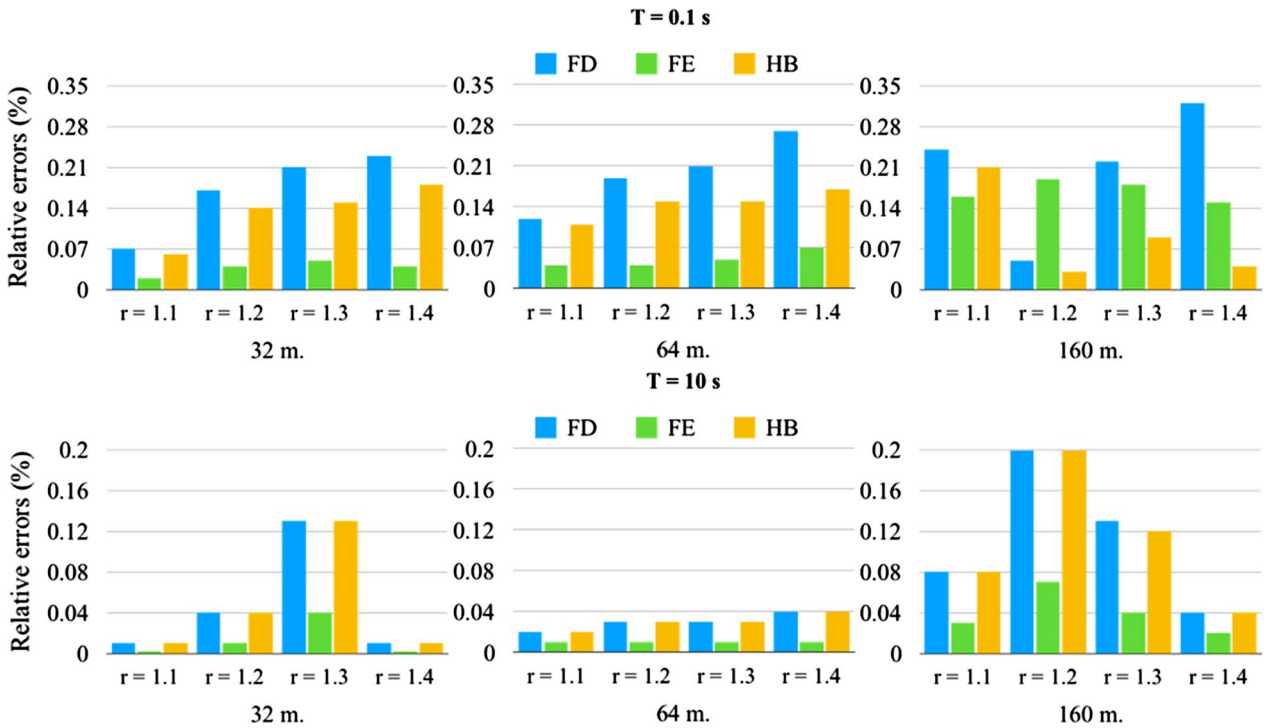

Fig. 7 Relative errors (%) of phases calculated at $T = 0.1$(top) and 10 s (bottom) for the two-layered model

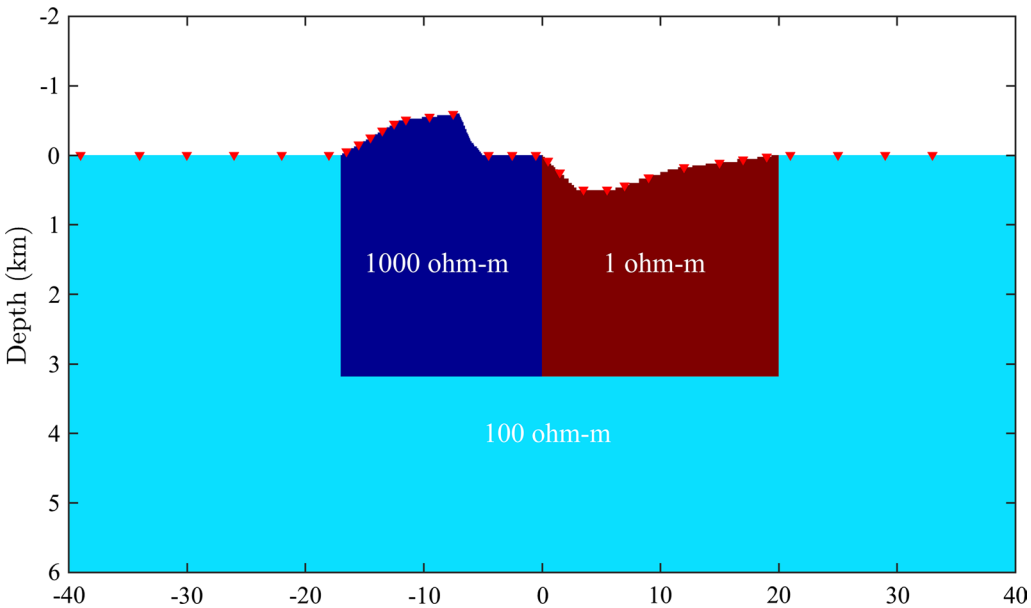

Fig. 8 Topographic model with mountain and valley (top). The sites marked as red triangles lie on the air–earth interface

mountain is 600 m, whereas the deepest part of the valley is 500 m. The size of the model is set as 100 km × 300 km. The 31 sites with different distances are spread over these topographic zones and some surrounding flat zones. The periods of the EM field used to calculate the responses are $T = 0.1, 1, 10$ and 100 s.

To compare the accuracy of the numerical schemes, the responses calculated by the FE method with a fine mesh are used as a benchmark. The fine mesh includes 47,952 elements and 48,675 nodes. The hybrid FD–FE and FE methods use the same mesh with 17,995 elements and 18,352 nodes. The number of FE nodes inserted in the hybrid FD–FE to cover topographic zone is only 2448, which is approximately 13% of the total nodes. Therefore, the number of nonzeros in the coefficient matrix of the hybrid FD–FE method increases by 9792 nonzeros compared with FD. The mesh for the FD method is quite different from those of the other methods. More refinement of the mesh is required to handle topography. The total numbers of rectangular blocks and nodes are 93,625 and 94,336, respectively. The comparison of the responses calculated for $T = 10$ s is shown in Fig. 9.

The hybrid FD–FE scheme provides responses that are very close to the benchmark as well as those of the FE method. For the FD method, some large discrepancies occur at a few sites, even though a very fine rectangular mesh is applied around the topographic zone. The total CPU times required to finish the task for 4 periods are shown in Fig. 10.

The hybrid FD–FE approach takes the shortest time to complete the task for 4 periods, whereas FD takes the longest time. Note that the FE with fine mesh is excluded in this comparison. These results indicate that the hybrid method is more powerful than the FE and FD methods when topography exists in the model.

Bathymetric model

The bathymetric model is shown in Fig. 11. The base of the flat seafloor is designed at a depth $z = 500$ m, and the resistivity of the sea is set as 0.2 ohm-m. The curve of bathymetry is designed by mixing Gaussian distribution functions. There are three types of trenches. The widest trench is located at left, the narrowest trench is located near the center, and the middle trench is located at right. The deepest part of the sea is 1.5 km. For the earth subsurface beneath the sea, two anomalies are buried in the

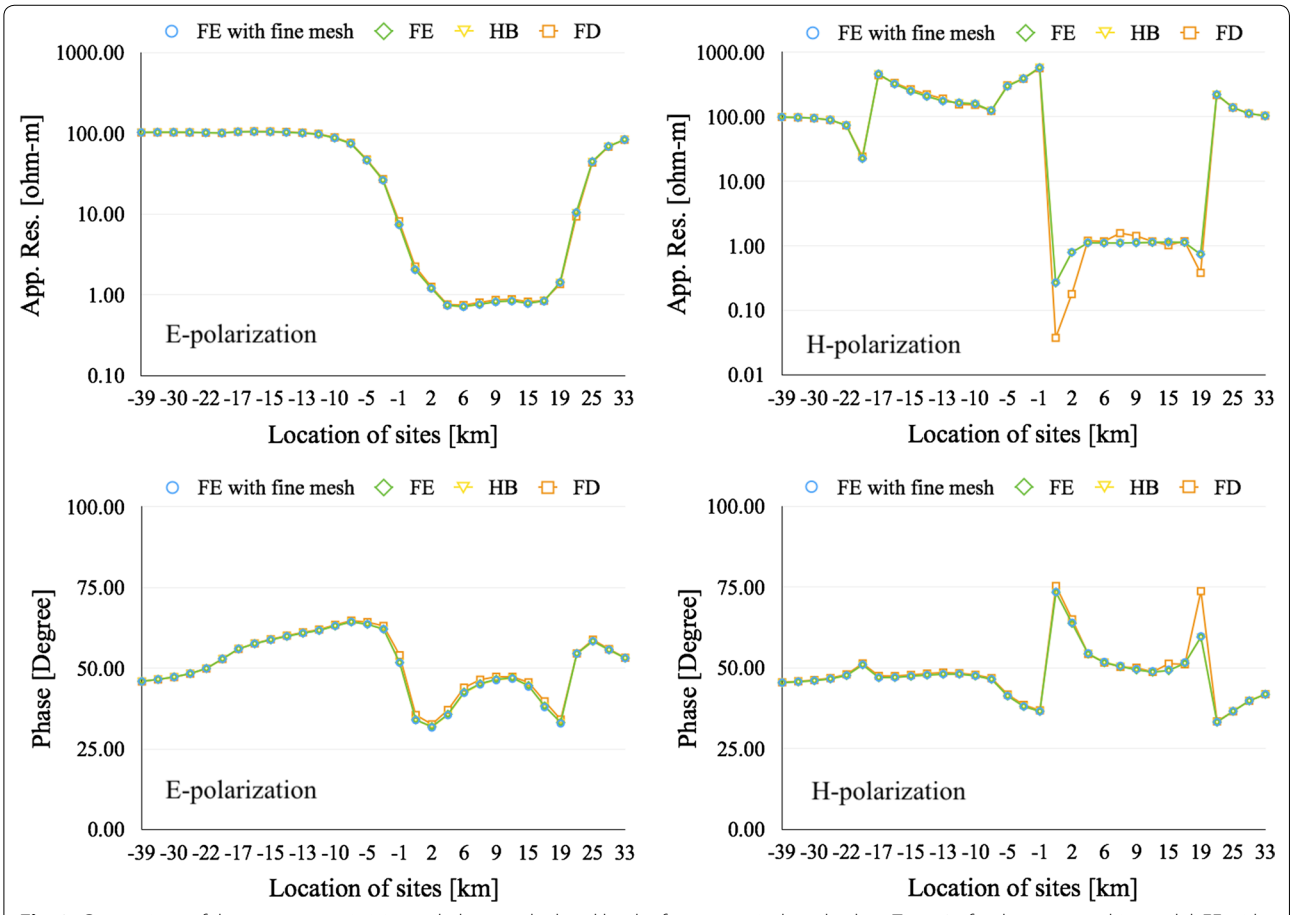

Fig. 9 Comparison of the apparent resistivity and phases calculated by the four numerical methods at $T = 10$ s for the topographic model: FE with fine mesh (circle), FE (diamond), HB (triangle) and FD (square) methods. The apparent resistivities for the *E*- and *H*-polarizations are at the left and right top, respectively, whereas the phases for the *E*- and *H*-polarizations are at the left and right bottom, respectively

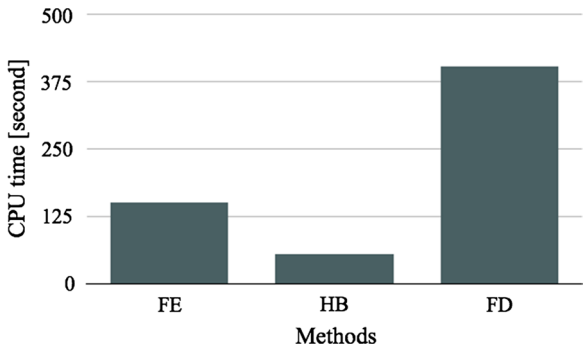

Fig. 10 The total CPU times required by the FE, HB and FD methods for the topographic model

100 ohm-m halfspace. The first one is a rectangular block with 5 ohm-m and a thickness of 500 m that extends from the center to the left boundary at a depth of 2 km. The other is a 5 km $\times$ 3.5 km rectangular block with 500 ohm-m that is buried at a depth of 2–5 km. The 20 sites with nonuniform distance are spread over this bathymetry and some portions of the flat seafloor. The periods of the EM field used to calculate the response are $T = 0.1, 1.0, 10$ and 100 s.

To compare the accuracy of the numerical schemes, the FE method with fine mesh includes 84,018 elements and 84,638 nodes. The hybrid FD–FE and FE methods use the same mesh with 25,132 elements and 25,461 nodes. Note that the vertical mesh in the sea layer is the same in the three schemes because the penetration depth of EM in this layer is reduced dramatically and affects the accuracy of these numerical schemes. The number of FE nodes inserted in the hybrid method in some parts of the sea layer and covering the bathymetric zone is approximately 6273 (approximately 25% of the total nodes). As a result, the number of nonzeros in the coefficient matrix of hybrid FD–FE increases, with 25,092 nonzeros. The mesh for the FD method is still quite different from those of the other methods. Refinement of the mesh is required to handle bathymetry. The total numbers of rectangular blocks and nodes are 104,832 and 105,501, respectively. The comparison of the responses calculated at $T = 1$ and 10 s is shown in Fig. 12.

The hybrid FD–FE scheme provides responses that are very close to those of the benchmark as well as those of the FE method. For the FD method, some large discrepancies occur at many sites, even though a very fine rectangular mesh is applied around the bathymetric zone, particularly for *H*-polarization. The total CPU times required to finish the task for 4 periods are shown in Fig. 13.

The hybrid FD–FE method still takes the shortest time to complete the task for 4 periods, whereas the FD method still takes the longest time. These results also indicate that the hybrid method is more powerful than the FE and FD methods when bathymetry exists in the model.

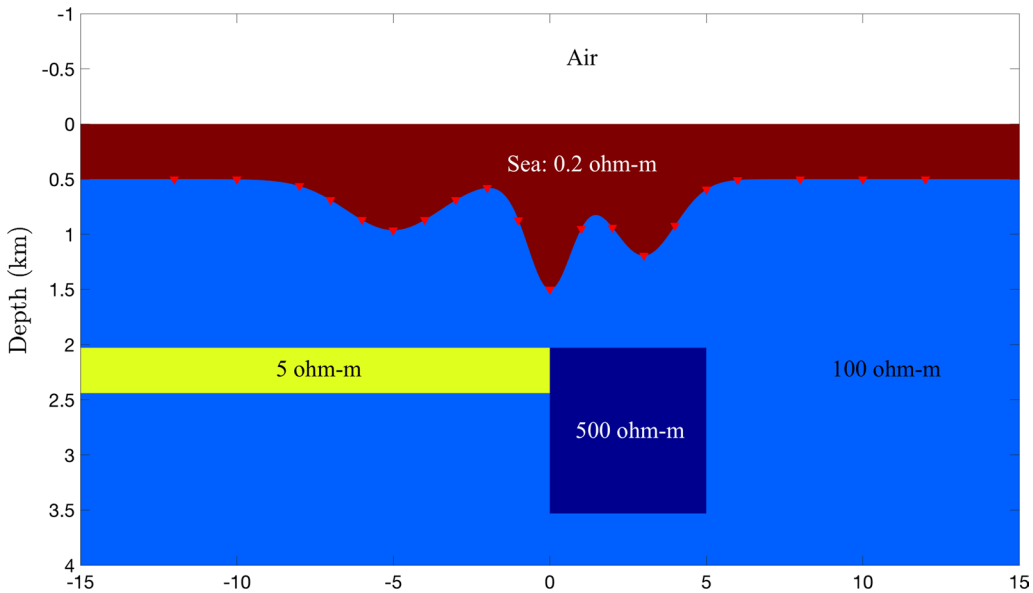

Fig. 11 Bathymetric model with mixing of Gaussian distribution functions. The sites marked as red triangles lie on the sea–earth interface

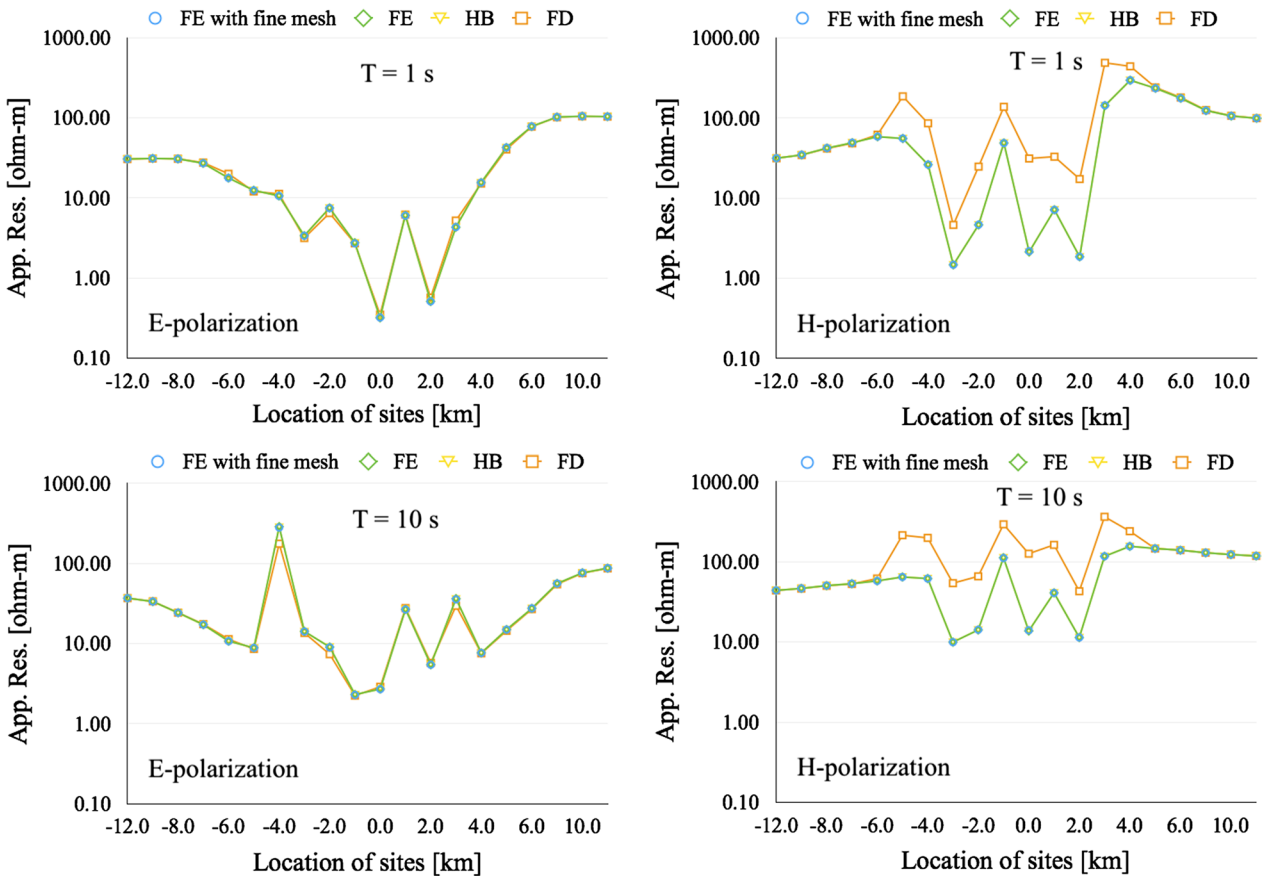

Fig. 12 The apparent resistivities computed at $T = 1$ s of the bathymetric model for the *E*- and *H*- polarizations are shown at the left and right top, respectively, whereas those computed at $T = 10$ s are shown at the left and right bottom, respectively

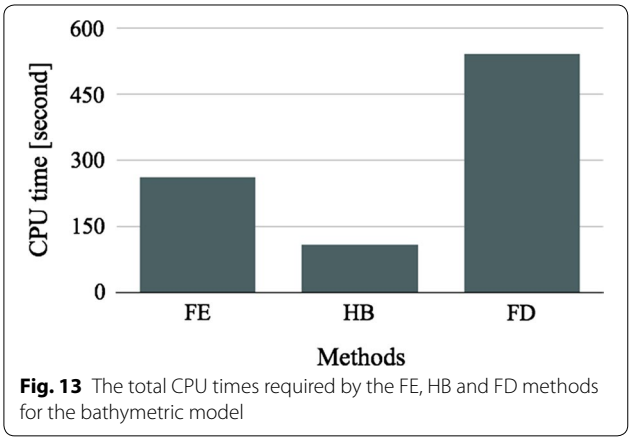

Fig. 13 The total CPU times required by the FE, HB and FD methods for the bathymetric model

Conclusions

In this paper, a hybrid FD–FE method is developed. The common FD method and the FE method with quadrilateral elements are used to construct the hybrid method. The FD method is applied in areas where topography and bathymetry do not exist. By contrast, the FE method is applied around topography and bathymetry zones. The characteristics of the resulting system of equations of 2-D magnetotelluric modeling are a combination of those of the FD and FE methods. The hybrid FD–FE method is validated and compared to the common FD and FE methods. The accuracy and efficiency of the hybrid method in terms of relative errors and memory storage and in terms of calculation time, respectively, are presented for various models, including nontopographic model with two layers, topographic models and bathymetric models. For nontopographic models, the efficiency and accuracy of the hybrid FD–FE method are close to those of the FD method. For topographic and bathymetric models, the hybrid FD–FE method can handle topography and bathymetry appropriately as well as the FE method. Furthermore, the hybrid FD–FE method can provide accuracy equivalent to the FE method, but the calculation is dramatically reduced compared to that of the FE scheme. By contrast, the FD method provides poor accuracy and

requires more calculation time even though a mesh with a huge number of nodes and blocks is used.

Based on these results, the hybrid method may represent a new, better option for the forward calculation routine for 2-D magnetotelluric inversion to interpret real field magnetotelluric data in the future. Note that the hybrid FD–FE method that has been presented uses a structured mesh. Some extra mesh refinement can appear in the projective subregion where topography or bathymetry exists. This extra mesh refinement will not appear when an unstructured quadrilateral mesh is applied in the FE zone instead. The unstructured quadrilateral mesh has a local refinement mesh as well as an unstructured triangular mesh but provides better accuracy without adaptive routines (Sarakorn 2017). The size of the elements around the boundary of the FE zone is optimized nearly equally. The connected rectangular blocks in the FD zone then have a conformal shape and a good edge ratio. Thus, the hybrid method is enhanced by this feature. However, some procedures, such as mesh generation and node and element numbering, need to be revisited and modified. Furthermore, the concept of the hybrid FD–FE method can be extended and applied to solve 3-D MT modeling in the future.

Authors' contributions

WS developed the theoretical concepts, performed the numerical simulations and contributed to the final version of the manuscript. CV supervised the project. Both authors read and approved the final manuscript.

Author details

[1] Department of Mathematics, Faculty of Science, Khon Kaen University, Khon Kaen 40002, Thailand. [2] Curl-E Geophysics Co. Ltd, 85/87 M. Nantawan Utthayan-Aksa Rd., Salaya, Phutthamonthon, Nakornpathom 73170, Thailand.

Acknowlegements

The authors also would like to thank Assoc. Prof. Dr. Weerachai Siripunvaraporn, Department of Physics, Faculty of Science, Mahidol University, for many useful suggestions for improving this research.

Competing interests

The authors declare that they have no competing interests.

Availability of data and materials

All the data and models in this manuscript are available.

Funding

This work has been supported by 1. The DPST Research grant (Grant Number 002/2557). 2. The Academic Affairs Promotion Fund, Faculty of Science, Khon Kaen University, Fiscal year 2560 (RAAPF). 3. The National Research Council of Thailand and Khon Kaen University, Thailand (Grant Number 6100148).

Publisher's Note

Received: 31 January 2018 Accepted: 14 June 2018
Published online: 26 June 2018

References

Baba K, Chave AD (2005) Correction of seafloor magnetotelluric data for topographic effects during inversion. J Geophys Res B Solid Earth 110(12):1–16
Egbert GD, Kelbert A (2012) Computational recipes for electromagnetic inverse problems. Geophys J Int 189(1):251–267
Erdoğan E, Demirci I, Candansayar ME (2008) Incorporating topography into 2D resistivity modeling using finite-element and finite-difference approaches. Geophysics 73(3):F135–F142
Franke A, Börner R-U, Spitzer K (2007) Adaptive unstructured grid finite element simulation of two-dimensional magnetotelluric fields for arbitrary surface and seafloor topography. Geophys J Int 171(1):71–86
Galis M, Moczo P, Kristek J (2008) A 3-D hybrid finite-difference–finite-element viscoelastic modelling of seismic wave motion. Geophys J Int 175(1):153–184
Grayver AV (2015) Parallel three-dimensional magnetotelluric inversion using adaptive finite-element method. Part I: theory and synthetic study. Geophys J Int 202(1):584–603
Grayver AV, Kolev TV (2015) Large-scale 3D geoelectromagnetic modeling using parallel adaptive high-order finite element method. Geophysics 80(6):277–291
Jianfeng Z, Tielin L (2002) Elastic wave modelling in 3D heterogeneous media: 3D grid method. Geophys J Int 150(3):780–799
Key K, Weiss C (2006) Adaptive finite-element modeling using unstructured grids: the 2D magnetotelluric example. Geophysics 71(6):G291–G299
Kordy M, Wannamaker P, Maris V, Cherkaev E, Hill G (2016a) 3-D magnetotelluric inversion including topography using deformed hexahedral edge finite elements and direct solvers parallelized on SMP computers—part I: forward problem and parameter jacobians. Geophys J Int 204(1):74–93
Kordy M, Wannamaker P, Maris V, Cherkaev E, Hill G (2016b) 3-dimensional magnetotelluric inversion including topography using deformed hexahedral edge finite elements and direct solvers parallelized on symmetric multiprocessor computers—part II: direct data-space inverse solution. Geophys J Int 204(1):94–110
Lee S, Kim H, Song Y, Lee C-K (2009) MT2DInvMatlab—a program in MATLAB and FORTRAN for two-dimensional magnetotelluric inversion. Comput Geosci 35(8):1722–1734
Mackie RL, Madden TR, Wannamaker PE (1993) Three-dimensional magnetotelluric modeling using difference equations—theory and comparisons to integral equation solutions. Geophysics 58(2):215–226
Matsuno T, Seama N, Baba K (2007) A study on correction equations for the effect of seafloor topography on ocean bottom magnetotelluric data. Earth Planets Space 59(8):981–986. https://doi.org/10.1186/BF03352037
Nam MJ, Kim HJ, Song Y, Lee TJ, Son J-S, Suh JH (2007) 3D magnetotelluric modelling including surface topography. Geophys Prospect 55(2):277–287
Nam MJ, Kim HJ, Song Y, Lee TJ, Suh JH (2008) Three-dimensional topography corrections of magnetotelluric data. Geophys J Int 174(2):464–474
Ren Z, Kalscheuer T, Greenhalgh S, Maurer H (2013) A goal-oriented adaptive finite-element approach for plane wave 3-D electromagnetic modelling. Geophys J Int 194(2):700–718
Sarakorn W (2017) 2-D magnetotelluric modeling using finite element method incorporating unstructured quadrilateral elements. J Appl Geophys 139:16–24
Schwalenberg K, Edwards R (2004) The effect of seafloor topography on magnetotelluric fields: an analytical formulation confirmed with numerical results. Geophys J Int 159(2):607–621
Sharma SP, Kaikkonen P (1998) An automated finite element mesh generation and element coding in 2-D electromagnetic inversion. Geophysica 34(3):93–114
Simpson M, Clement T (2003) Comparison of finite difference and finite element solutions to the variably saturated flow equation. J Hydrol 270(1):49–64
Singer BS (1992) Correction for distortions of magnetotelluric fields: limits of validity of the static approach. Surv Geophys 13(4):309–340
Siripunvaraporn W, Egbert G, Lenbury Y (2002) Numerical accuracy of magnetotelluric modeling: a comparison of finite difference approximations. Earth Planets Space 54(6):721–725. https://doi.org/10.1186/BF03351724

Usui Y (2015) 3-D inversion of magnetotelluric data using unstructured tetrahedral elements: applicability to data affected by topography. Geophys J Int 202(2):828–849

Usui Y, Ogawa Y, Aizawa K, Kanda W, Hashimoto T, Koyama T, Yamaya Y, Kagiyama T (2017) Three-dimensional resistivity structure of Asama Volcano revealed by data-space magnetotelluric inversion using unstructured tetrahedral elements. Geophys J Int 208(3):1359–1372

Usui Y, Kasaya T, Ogawa Y, Iwamoto H (2018) Marine magnetotelluric inversion with an unstructured tetrahedral mesh. Geophys J Int 214(2):952–974

Vachiratienchai C, Boonchaisuk S, Siripunvaraporn W (2010) A hybrid finite difference–finite element method to incorporate topography for 2D direct current (DC) resistivity modeling. Phys Earth Planet Inter 183(3):426–434

Wannamaker PE, Stodt JA, Rijo L (1986) Two-dimensional topographic responses in magnetotellurics modeled using finite elements. Geophysics 51(11):2131–2144

Wannamaker PE, Stodt JA, Rijo L (1987) A stable finite element solution for two-dimensional magnetotelluric modelling. Geophys J R Astron Soc 88(1):277–296

Zhdanov MS, Varentsov IM, Weaver JT, Golubev NG, Krylov VA (1997) Methods for modelling electromagnetic fields results from COMMEMI—the international project on the comparison of modelling methods for electromagnetic induction. J Appl Geophys 37(3–4):133–271

Zienkiewicz O, Cheung Y (1965) Finite element in the solution of field problems. Engineering 220:507–510